Chinese Chemical Letters 34 (2023) 108164

Contents lists available at ScienceDirect

Chinese Chemical Letters

journal homepage: www.elsevier.com/locate/cclet

3D anchoring structured for $LiFe_{0.5}Mn_{0.5}PO_4$@cornstalk-C cathode materials

Guangliang Zhang[a], Riran Zang[a], Man Mo[b], Zhijie Fang[b], Yangxian Huang[c], Kunsong Hu[c], Jiali Huang[d], Xinxiang Liu[d], Lingyun Huang[d], Guohui Kang[d], Weijian Li[e], Haiqing Zhan[e], Xianquan Ming[e], Guanhan Huang[e], Guiliang Li[e], Feng Zhan[a,*]

[a] School of Resources Environment and Materials, Guangxi University, Nanning 530004, China
[b] School of Electronics Engineering, Guangxi University of Science and Technology, Liuzhou 545006, China
[c] State Key Laboratory of Featured Metal Materials and Life-cycle Safety for Composite Structures, Guangxi University, Nanning 530004, China
[d] Guangxi Higher Education Key Laboratory of High Performance Structural Materials and Heat Treatment & Surface Processing, Guangxi University, Nanning 53004, China
[e] South Manganese Group Limited, Nanning 530029, China

ARTICLE INFO

Article history:
Received 16 December 2022
Revised 10 January 2023
Accepted 26 January 2023
Available online 28 January 2023

Keywords:
$LiFe_{0.5}Mn_{0.5}PO_4$
Cornstalk
Solvothermal method
3D anchoring structure
Cathode materials

ABSTRACT

The organic carbon source coating $LiFe_xMn_{1-x}PO_4$ suffers from the problem of non-uniform carbon cladding. Too thick carbon cladding layer instead hinders the de-embedding of lithium ions. In this paper, we choose cornstalk as the carbon source, then $LiFe_{0.5}Mn_{0.5}PO_4$@cornstalk-C (LFMP@C-C) with 3D anchoring structure is prepared by the solvothermal method. The results show that the LFMP with cornstalk as the carbon source has better performance compared to the sucrose-coated LFMP material (LFMP@C). The discharge capacity of LFMP@C-C is 116 mAh/g for the first cycle at 1 C and the capacity retention rate is 94.0% after 500 cycles, and the discharge capacity of LFMP@C-C is more than 17.17% higher than that of LFMP@C.

Among lithium-ion batteries, olivine-structured $LiFe_xMn_{1-x}PO_4$ combines the advantages of $LiFePO_4$ and $LiMnPO_4$ [1–3], but still has the disadvantages of low electronic conductivity and low ion mobility. Currently, the material's electronic conductivity and ion mobility is mainly improved through carbon coating [4,5]. Besides, the carbon framework can effectively buffer the volume swelling during discharge and charging processes [6,7]. The carbon source of carbon coating is mainly organic compounds such as sucrose, glucose, polyaniline. The carbon coating still has the problem of non-uniformity, which can affect the transport of lithium ions and reducing the amount of $LiFe_xMn_{1-x}PO_4$ participate in the redox reaction during charging and discharging [8]. As a renewable resource, plants contain a large number of internal voids for transporting and storing water, and biomass carbon materials with abundant voids can be prepared through high-temperature carbonization. Biomass carbon is simple to prepare, environmentally friendly, low cost, and abundant in raw materials [9,10]. Because of its graphene-like structure and unique rich void structure, it can provide a three-dimensional conductive network in battery materials and improve the electron conductivity and ion mobility of materials, thus improving the cycle stability of lithium-ion batteries [11–13].

In this paper, cornstalk was selected as the biomass carbon source, and the ellipsoidal LFMP was prepared by the solvothermal method. $LiFe_{0.5}Mn_{0.5}PO_4$ (LFMP) particles were uniformly attached to the pretreated cornstalk powder by ultrasonic method, and the $LiFe_{0.5}Mn_{0.5}PO_4$@cornstalk-C (LFMP@C-C) lithium-ion battery cathode material with 3D anchoring structure was prepared by high-temperature sintering [14]. The synthesized material was characterized by X-ray diffraction (XRD, 10°–80°) and scanning electron microscopy (SEM). Electrochemical tests were performed on the LFMP@C-C and the sucrose-coated LFMP material (LFMP@C).

Appropriate amounts of $LiOH{\cdot}H_2O$ (Adamas-beta, AR), H_3PO_4 (GHTECH, AR), $MnSO_4{\cdot}H_2O$ (GENERAL-REAGENT, AR), and $FeSO_4{\cdot}7H_2O$(GENERAL-REAGENT, AR) were weighed according to the molar ratio of 6:2:1:1, and thus added to the mixed solvent of deionized water and ethylene glycol (1:1, v/v) with constant stirring, and added a certain amount of surfactant (CTAB, GENERAL-REAGENT, AR) and ascorbic acid, stirred vigorously for 3 h, transferred the mixed solution into the PTEF autoclave, passed argon gas for 5 min, held in the oven at 180 °C for 18 h, and waited

* Corresponding author.
E-mail address: phy_idea@outlook.com (F. Zhan).

https://doi.org/10.1016/j.cclet.2023.108164
1001-8417/

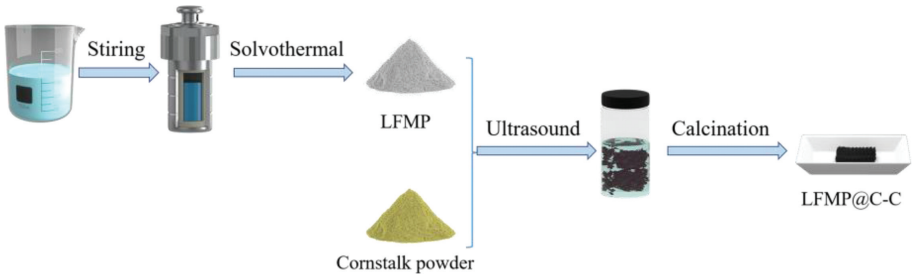

Fig. 1. Schematic illustration of the fabrication process of LFMP@C-C.

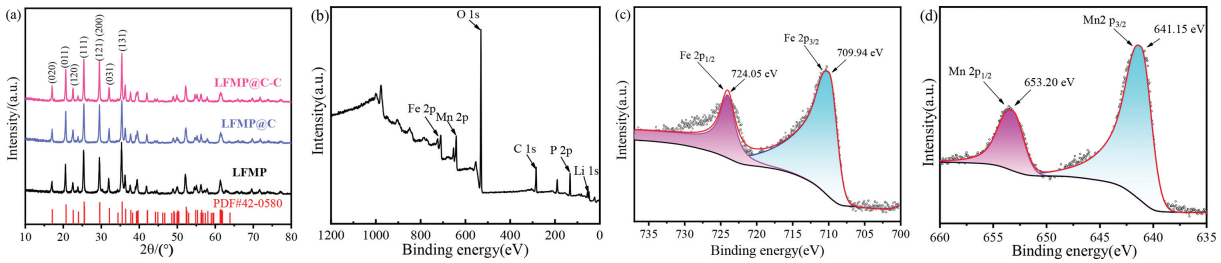

Fig. 2. (a) XRD patterns of LFMP, LFMP@C-C and LFMP@C. XPS spectra of the LFMP: (b) XPS survey spectrum, (c) high-resolution Fe 2p spectra, (d) high-resolution Mn 2p spectra.

for cooling to room temperature naturally, the autoclave was opened and the precipitate obtained was collected by centrifugation, washed with deionized water and ethanol alternately for 6 times, and the obtained product was dried in an oven at 80 °C to obtain LFMP material. The pretreated cornstalk powder was mixed with LFMP powder in alcohol solution by sonication for 4 h, dried at 40 °C for 24 h, and then put into a tube furnace at 700 °C for 4 h to obtain LFMP@C-C cathode material. The preparation flow chart is shown in Fig. 1.

The samples were characterized by X-ray powder diffraction (XRD, D/MAX2500V, Rigaku, Japan), X-ray photoelectron spectroscopy (XPS, ESCALAB 250XI+, Thermo Fisher Scientific, US) and scanning electron microscopy (SEM, SU8020, Hitachi, Toyo, Chiba, Japan).

The electrodes were prepared by mixing active materials with Super P and PVDF (Adamas-beta, RG) binder at a weight ratio of 75:15:10. The obtained slurry was coated on aluminum foil and dried at a vacuum oven at 120 °C for 12 h The coin cell were assembled with LBC6300 (1 mol/L $LiPF_6$ dissolved in EC:EMC:DEC (1:1:1)) as the electrolyte, lithium metal pellets as the negative electrode, and polypropylene microporous film as the diaphragm, and the CR2032 coin cells were assembled in a glove box filled with argon gas.

The CV tests and the electrochemical impedance spectroscopy (EIS) tests were carried out on an electrochemical workstation (CHI760E, CH Instruments Ins) before the charge-discharge test. The voltage scan range for the CV test was 2.2–4.7 V with a scan rate of 0.1 mV/s; the test range for the EIS was 0.01–10^5 Hz with a perturbation voltage of 0.005 V. The charge-discharge measurements were conducted on a battery test system (BTS-5V10mA, Shenzhen NEWARE), at room temperature in the 2–4.7 V range in the constant voltage mode.

Fig. 2a shows the XRD patterns of LFMP, LFMP@C-C and LFMP@C. The diffraction peaks of the three samples match with the standard card (PDF#42–0580) of the $LiFe_{0.5}Mn_{0.5}PO_4$ sample. No impurity peaks are observed and the peaks are sharp, indicating the high purity and crystallinity of the samples. In addition, the highest diffraction peaks of LFMP, LFMP@C and LFMP@C-C are observed at the (131) crystal plane, which are consistent with the standard card. The $I(020)/I(200)$ values of LFMP, LFMP@C and LFMP@C-C are 0.360, 0.373 and 0.405, respectively, which are larger than the standard card (0.340), indicating that the samples have a large number of (010) crystal plane exposed in the olivine structure material. The exposed (010) crystal plane on the surface of the olivine structured samples can reduce the diffusion distance of Li^+ ion and provide a large number of active sites for the diffusion of Li^+ ion. LMFP@C-C has a higher $I(020)/I(200)$ value compared to LMFP@C, indicating a faster Li^+ ion transport capacity during charge/discharge.

The XPS full spectra of LFMP is shown in Fig. 2b, the spectral lines of Li, Fe, Mn, P and O elements in the LFMP samples could be found in the full spectra. Due to spin-orbit coupling, Fe 2p consists of two parts, Fe $2p_{3/2}$ and Fe $2p_{1/2}$, each consisting of the main peak and a satellite peak, and the oxidation state of Fe is mainly related to the position of the binding energy of the main peak. For the Fe^{2+} ion in $LiFePO_4$, the main peaks of Fe $2p_{3/2}$ and Fe $2p_{1/2}$ are located at 710.5 and 724 eV, respectively. For the Fe^{3+} ion in $FePO_4$, the main peaks of Fe^{3+} ions in $FePO_4$, Fe $2p_{3/2}$ and Fe $2p_{1/2}$ are located at 712.5 and 726 eV, respectively [15]. The position of the main peak of Fe 2p in Fig. 2c is consistent with the peak of Fe^{2+} ions, and the presence of Fe^{3+} ions was not detected. Fig. 2d shows the XPS spectrum of Mn 2p, the characteristic peaks with binding energies of 653.20 eV and 641.15 eV obtained by fitting correspond to Mn $2p_{3/2}$ and Mn $2p_{1/2}$, respectively, which are consistent with the divalent Mn ions, so that in the $LiFe_{0.5}Mn_{0.5}PO_4$ sample, the oxidation states of both Fe and Mn are +2 valence [16].

The SEM images of LFMP@C-C and LFMP@C are shown in Fig. 3, from which it can be seen that the LFMP produced by the hydrothermal method is ellipsoidal particles of about 150 nm in length and 100 nm in width with uniform particle size distribution. This is due to the presence of CTAB, which shortens the size of lithium manganese iron phosphate particles in the b-axis direction and effectively shortens the diffusion channel of Li^+ [17,18]. From Figs. 3a and b, it is observed that the carbonized cornstalk is a folded flake porous structure, and the lithium iron phosphate nanoparticles are uniformly anchored on the folded flake layer so that the lithium iron phosphate particles are uniformly arranged on the carbon layer of cornstalk according to the b-axis direction perpendicular to the flake layer, which forms a 3D anchoring structure. From Figs. 3c and d, it is found that the LFMP@C is covered

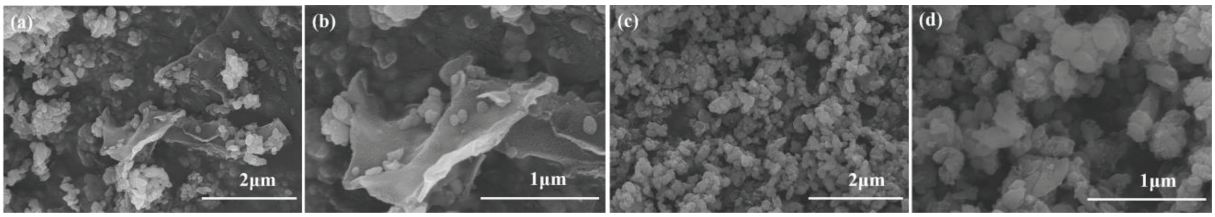

Fig. 3. (a, b) SEM image of the LFMP@C-C sample. (c, d) SEM image of the LFMP@C sample.

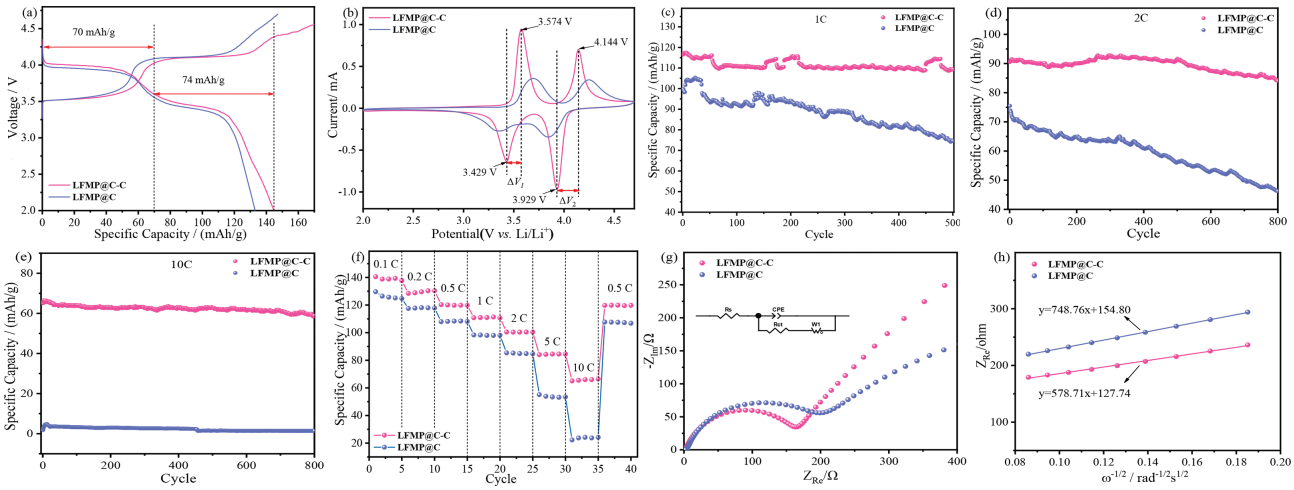

Fig. 4. (a) First charge−discharge profiles at 0.1 C. (b) CV curves at a scan rate of 0.1 mV/s of LMFP@C-C and LMFP@C. Cycling performance of LMFP@C-C and LMFP@C: (c) at 1 C, (d) at 2 C, (e) at 10 C. (f) Rate performance of LMFP@C-C and LMFP@C. (g) Nyquist impedance spectra and equivalent circuit of LMFP@C-C and LMFP@C. (h) The relationship between Z_{Re} and $\omega^{-1/2}$ in the low frequency region.

with a slight agglomeration, and the small particles are attached to the surface of the large particles.

Fig. 4a shows the initial charge/discharge curves of LFMP@C-C and LFMP@C materials. Both have two voltage plateaus at 3.5 V and 4.1 V, corresponding to the redox pairs with Fe^{2+}/Fe^{3+} and Mn^{2+}/Mn^{3+}. the specific capacity of LFMP@C-C for discharge is 144 mAh/g, where the 3.5 V plateau (Fe^{2+}/Fe^{3+}, 70 mAh/g) and the 4.1 V plateau (Mn^{2+}/Mn^{3+}, 74 mAh/g) contribute a capacity ratio of 0.48:0.52, which is close to 1:1. The discharge specific capacity of LFMP@C is 133 mAh/g, which is 11 mAh/g lower than that of LFMP@C-C. This is due to the agglomeration of the primary sucrose-coated lithium manganese iron phosphate material and the uneven sucrose carbon coating, and the inhomogeneous carbon coating layer affects the lithium-ion transport instead [19]. Fig. 4b shows the cyclic voltammetry test performed on the material, and two pairs of obvious redox peaks can be seen for Fe^{2+}/Fe^{3+} and Mn^{2+}/Mn^{3+} redox reactions, which correspond to the charge/discharge curves and are accompanied by the process of lithium-ion detachment and embedding, respectively. Compared with the LFMP@C cathode material, the LFMP@C-C cathode material exhibits strong and sharp redox peaks with smaller redox potential differences (The peak voltage differences ΔV_1 and ΔV_2 for Fe^{2+}/Fe^{3+} and Mn^{2+}/Mn^{3+} of LFMP@C-C are 145 mV and 215 mV, respectively. The peak voltage differences ΔV_1 and ΔV_2 for Fe^{2+}/Fe^{3+} and Mn^{2+}/Mn^{3+} of LFMP@C are 324 mV and 401 mV, respectively.), which indicates that the LFMP@C-C cathode material has better electrochemical properties as well as smaller polarization. Moreover, the two teams of redox peaks of LFMP@C-C cathode material have good symmetry, which indicates that the material has good reversibility during the charging and discharging process.

Fig. 4c shows the cycling performance of LFMP@C-C and LFMP@C at 1 C, from which it can be seen that the LFMP@C-C material has the better cycling performance. The discharge specific capacity of LFMP@C-C material is 116 mAh/g for the first discharge and 109 mAh/g after 500 cycles of the material, with a capacity retention rate of 94.0%. The capacity retention rate of LFMP@C is only 74.7% (the discharge specific capacities of the first and 500th turns of LFMP@C are 99 and 74 mAh/g, respectively). Figs. 4d and e show the cycling performance of LFMP@C-C and LFMP@C at 2 C and 10 C. Compared with LFMP@C, LFMP@C-C materials still have better cycling performance at high rates, especially at 10 C rate, the discharge specific capacity of LFMP@C-C is 65 mAh/g, while the discharge specific capacity of LFMP@C is only 2 mAh/g. Fig. 4f shows the comparison of the rate performance of LFMP@C-C and LFMP@C. As expected, the LMFP@C-C exhibits higher rate capability. It presents discharge specific capacities of 140, 128, 120, 110, 100, 84 and 65 mAh/g at 0.1, 0.2, 0.5, 1, 2, 5 and 10 C rate, respectively, while LMFP@C are 129, 117, 107, 98, 85, 55 and 22 mAh/g at the same current density. Notably, after charging/discharging at a high current rate of 10 C, the specific capacity of LMFP@C-C can still recover to 119 mAh/g when the rate is regained at 0.5 C, revealing it has superior high current density tolerance capability.

Fig. 4g shows the impedance diagram of the cathode material and the equivalent circuit diagram. The inset shows the corresponding equivalent circuit to fit the AC impedance of the sample for the analysis. R_s, CPE, R_{ct} and W_1 are the electrolyte resistance, dual capacitance, charge transfer impedance, and solid phase diffusion resistance, respectively. As shown in Table S1 (Supporting information), the LFMP@C with a charge transfer impedance R_{ct} value of 219.2 Ω, the charge transfer impedance R_{ct} value of the LFMP@C-C is 172.9 Ω, indicates that the LFMP@C-C cathode material has a smaller Li^+ ion diffusion impedance.

The slope of Z_{Re} *versus* ω is calculated by Eq. S2 (Supporting information) and Fig. 4h, *i.e.*, σ. Then the lithium-ion diffusion coefficient of the material is calculated by Eq. S1 (Supporting infor-

mation), as shown in Table S1. Accordingly, the apparent Li^+ ion diffusion coefficients of LMFP@C-C and LMFP@C are determined to be 1.71×10^{-13} and 1.02×10^{-13}, respectively. The greater Li^+ ion diffusion coefficient of LFMP@C-C is consistent with its better electrochemical properties.

In conclusion, the LFMP@C-C materials with 3D anchoring structure were prepared. The folded lamellar structure of cornstalk carbon provides a three-dimensional conductive network for LFMP. LFMP nanoparticles are uniformly arranged in the direction of the b-axis perpendicular to the carbon layer, which has faster lithium-ion diffusion and electron transfer capability compared with sucrose coating, and thus the LFMP@C-C cathode materials have excellent electrochemical performance in terms of specific capacity and cycling performance. The discharge-specific capacity is 116 mAh/g in the first cycle of 1 C and 109 mAh/g after 500 cycles of the material, with a capacity retention rate of 94.0%. We also compared our experiments with those of others before us [20,21]. The cornstalk we used is environmentally friendly, low cost and rich in raw materials. Our samples have a special structure that is better for lithium ion diffusion. The discharge capacity of our samples is 5.45% higher than that of theirs, and the capacity retention rate is more than 2.22% higher than theirs. This is good news for the development of LFMP. In the future, we will further optimize the preparation process to achieve industrial production.

Declaration of competing interest

The authors declare that they have no known competing financial interests or personal relationships that could have appeared to influence the work reported in this paper.

Acknowledgments

This work was supported by CITIC Dameng Mining Industries Limited-Guangxi University Joint Research Institute of manganese resources utilization and advanced materials technology, Guangxi University-CITIC Dameng Mining Industries Limited Joint base of postgraduate cultivation, National Natural Science Foundation of China (No. 11364003), Guangxi Innovation Driven Development Project (Nos. AA17204100, AA18118052), the Natural Science Foundation of Guangxi Province (No. 2018GXNSFAA138186)

Supplementary materials

Supplementary material associated with this article can be found, in the online version, at doi:10.1016/j.cclet.2023.108164.

References

[1] F. Jiang, K. Qu, M. Wang, et al., Sustain. Energy Fuels 4 (2020) 2741–2751.
[2] Y. Liu, Y.J. Gu, J.L. Deng, et al., J. Mater. Sci. Mater. Electron. 31 (2020) 2887–2894.
[3] J. Ding, Z. Su, H.L. Tian, Ceram. Int. 42 (2016) 12435–12440.
[4] H. Yu, Z. Yang, H. Zhu, H. Jiang, C. Li, Chin. J. Chem. Eng. 28 (2020) 1935–1940.
[5] J.L. Liu, W.J. Liao, A.S. Yu, J. Alloys Compd. 587 (2014) 133–137.
[6] Q. Deng, X. Liu, Z. Li, et al., J. Colloid Interface Sci. 633 (2023) 480–488.
[7] X. Li, H. Liang, B. Qin, et al., J. Colloid Interface Sci. 625 (2022) 41–49.
[8] G.N. Zhu, C.X. Wang, Y.Y. Xia, J. Electrochem. Soc. 158 (2011) A102–A109.
[9] H.Q. Zhao, Y. Cheng, W. Liu, et al., Nano Micro Lett. 11 (2019) 24.
[10] J.C. Arrebola, A. Caballero, L. Hernan, et al., J. Electrochem. Soc. 157 (2010) A791–A797.
[11] J. Wang, P. Nie, B. Ding, et al., J Mater. Chem. A 5 (2017) 2411–2428.
[12] J. Liu, H. Yuan, X.Y. Tao, et al., EcoMat 2 (2020) e12019.
[13] P. Liu, Y. Wang, J. Liu, J. Energy Chem. 34 (2019) 171–185.
[14] Q. Deng, M. Wang, X. Liu, et al., J. Colloid Interface Sci. 626 (2022) 700–709.
[15] R.R. Zhao, B.Y. Lan, H.Y. Chen, G.Z. Ma, Ionics 18 (2012) 873–879.
[16] D. Choi, J. Xiao, Y.J. Choi, et al., Energy Environ. Sci. 4 (2011) 4560–4566.
[17] G.R. Du, X.Y. Guo, W.C. Yang, et al., J. Nanoparticle Res. 17 (2015) 272.
[18] Z.W. Deng, Q. Wang, D.C. Peng, H.B. Liu, Y.X. Chen, J. Alloys Compd. 794 (2019) 178–185.
[19] Z.X. Chi, W. Zhang, X.S. Wang, et al., J Mater. Chem. A 2 (2014) 17359–17365.
[20] Y. Yang, X. Chen, Y. Gu, et al., Mater. Lett. 299 (2021) 130053.
[21] N.V. Kosova, O.A. Podgornova, A.K. Gutakovskii, J. Alloys Compd. 742 (2018) 454–465.